sustainability

MDPI

Article

Bearing Characteristics of Deep Cement Mixing Integrated Drilling, Mixing and Jetting Piles Based on Numerical Simulation

Yang Wang [1], Yuhe Zhang [2], Kaixing Zhang [3], Yu Rong [2], Runze Xu [3], Jie Li [1], Weizhe Feng [4], Zihan Sang [2], Zhanyong Yao [2] and Kai Yao [2,5,*]

[1] Shandong Hi-Speed Construction Management Group Co., Ltd., Jinan 250300, China; wangyang92730@163.com (Y.W.); happiness@88.com (J.L.)
[2] School of Qilu Transportation, Shandong University, Jinan 250002, China; 202235471@mail.sdu.edu.cn (Y.Z.); 202015372@mail.sdu.edu.cn (Y.R.); 202335511@mail.sdu.edu.cn (Z.S.); zhanyong-y@sdu.edu.cn (Z.Y.)
[3] Shandong Hi-Speed Jinan Ring Road West Highway Co., Ltd., Jinan 250300, China; zhanggeoresearch@163.com (K.Z.); dxhxmb@163.com (R.X.)
[4] Shandong Provincial Communications Planning and Design Institute Group Co., Ltd., Jinan 250001, China; fengweiz@foxmail.com
[5] Shenzhen Research Institute of Shandong University, Shenzhen 518057, China
* Correspondence: yaokai@sdu.edu.cn; Tel.: +86-187-5313-7653

Abstract: The Deep Cement Mixing Integrated Drilling, Mixing and Jetting (DMJ) technique has been developed through the installation of high-pressure spray holes at the mixing blades, with the objective of enhancing the bearing capacity of deep-mixed piles in the Yellow River floodplain. In order to enhance the bearing capacity of the foundation, variable-modulus piles and capped piles were incorporated within the DMJ piles. Engineering applications have demonstrated that DMJ piles can effectively address the issue of foundation reinforcement in the Yellow River floodplain region, minimize the wastage of cement, and reduce the environmental pollution associated with waste slurry. Nevertheless, a comprehensive study of the relevant factors is still lacking in the available literature. This study addresses this gap by conducting a numerical simulation of these two types of DMJ piles based on the preliminary field test data, with the objective of analyzing both the single-pile-bearing characteristics and the composite foundation-bearing characteristics. Furthermore, the study seeks to optimize the DMJ pile's structure based on the simulation results. The findings demonstrate that the premature failure of a single pile during the bearing process can be averted if the modulus of the pile core reaches a minimum of 0.3 GPa or if the pile cap thickness exceeds 1 m. The utilization of large-diameter drilling, stirring and spraying piles can markedly enhance the bearing capacity of the composite foundation and mitigate the differential settlement of pile and soil. The spacing of the pile has been identified as a significant factor influencing the differential settlement of pile and soil. Consequently, this study also examines the impact of pile spacing on the differential settlement of piles and soil.

Keywords: deep mixing; Yellow River floodplain; numerical simulation; bearing characteristics; composite foundation; sustainable reinforcement

Citation: Wang, Y.; Zhang, Y.; Zhang, K.; Rong, Y.; Xu, R.; Li, J.; Feng, W.; Sang, Z.; Yao, Z.; Yao, K. Bearing Characteristics of Deep Cement Mixing Integrated Drilling, Mixing and Jetting Piles Based on Numerical Simulation. *Sustainability* **2024**, *16*, 9198. https://doi.org/10.3390/su16219198

Academic Editor: Manuela Almeida

Received: 21 August 2024
Revised: 7 October 2024
Accepted: 17 October 2024
Published: 23 October 2024

1. Introduction

In recent years, there has been a notable increase in the construction of highways, with foundation reinforcement representing a crucial aspect of this process. Deep cement mixing (DCM) [1] is the most prevalent method of foundation reinforcement [2]. Conventional deep mixing piles utilize the unidirectional rotation of the auger [3] to force the mixing of the reinforcing material and the on-site soil, forming higher-strength deep cement mixing piles. This is carried out with the aim of improving the bearing capacity of the foundation [4] and reducing deformation [5]. However, the traditional method often presents issues such as an uneven quality of the deep cement mixing piles and difficulty in achieving

a synergistic action between the piles and the soil. This results in a low bearing capacity of the foundations and a high susceptibility to safety hazards during the project.

The following pictures are taken from the foundation reinforcement of one highway in the Yellow River floodplain area (see Figures 1 and 2).

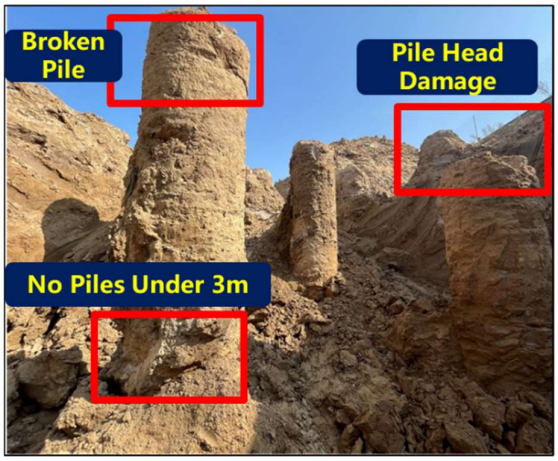

Figure 1. Upper part of the pile of conventional deep mixing technology.

Figure 2. Coring of conventional deep mixing techniques.

Conversely, a substantial body of engineering research has demonstrated that the conventional deep mixing technique results in the generation of considerable quantities of waste slurry in the Yellow River floodplain region. The improper disposal of this waste slurry leads to a significant loss of cement material and the contamination of the surrounding environment (see Figure 3).

Figure 3. Slurry bubbling in conventional deep mixing techniques.

The Yellow River floodplain is a distinctive geographical feature in China, the formation of which was caused by the flooding of the Yellow River. The strata of the Yellow River floodplain are deposited by the sediment of the Yellow River during flooding, and its stratigraphy and soil quality exhibit distinctive characteristics of a soft foundation. The soft soil found in the Yellow River floodplain is frequently interbedded with silt and clay. When subjected to natural consolidation, it readily forms a clay layer with a low water content, high degree of consolidation, and high strength. This contrasts with the behavior of sea-phase and lake-phase soft soils, which exhibit high water content and a state of soft plasticity and fluid plasticity.

The conventional deep mixing technique employs a low slurry pressure, which presents a challenge in forming piles in the typical silt and clay interbedded tectonic strata observed in the Yellow River floodplain. A number of researchers have presented a variety of approaches that have been investigated in order to address these issues [6–8]. In response to the advancement of construction equipment, Liu et al. [9]. conducted research on the bidirectional mixing pile and its construction process, subsequently developing the requisite supporting construction machinery. Fudo Tetra [10] developed the Jet and Churning System Management (JACSMAN) system, which is designed to counteract the pressure at the end of a high-pressure jet, thereby controlling the diameter of the pile. Bidirectional mixing technology and JACSMAN technology have resolved some of the issues pertaining to the quality of mixing piles. However, these two technologies are not without their own sets of challenges, including a complex equipment structure and a relatively low construction efficiency. Furthermore, in areas characterized by a complex soil distribution, such as the Yellow River floodplain [11], the phenomenon of pile immobility in highly consolidated clay layers [12,13] is frequently observed, which makes it exceedingly difficult to drill down and lift up the piles [14].

In order to address the engineering challenges associated with deep mixing technology in the Yellow River floodplain, two distinct types of DMJ piles have been developed. DMJ piles, otherwise known as drilling, mixing and jetting piles, employ high-pressure jetting (10–20 MPa) and relocation of the jetting nozzle from the drill pipe to the extremity of the mixing blades.

The deep cement mixing method, which integrates drilling, mixing and high-pressure jetting (DMJ), represents a novel approach to the reinforcement of weak strata in the Yellow River floodplain. The method relies on the use of small-diameter nozzles on the drill pipe to facilitate the mixing of the slurry into the soil layer, thereby forming a pile with a high-strength cylinder wall and a low-strength cylinder core. In terms of bearing characteristics, the essence of pile load transfer can be defined as the process of relative displacement of the pile-soil system, which generates resistance on the pile's outer side [15] and pile end resistance. In order to enhance the load-bearing capacity of the piles, new variable-modulus piles and capped piles were developed under the DMJ pile technique. The primary bearing area of deep mixing piles is the upper portion of the pile body, which is primarily supported by friction between the exterior of the pile body and the surrounding soil. In order to reduce the quantity of cement required, DMJ piles are designed with a high-strength outer layer and a low-strength inner layer. Additionally, to guarantee the bearing capacity of the upper portion of the pile body, DMJ piles are constructed with a top capping.

The results of field tests have demonstrated that DMJ piles are an effective method for improving the quality of foundation reinforcement. In comparison with conventional deep mixing technology, the quality and uniformity of pile formation are markedly enhanced by the use of DMJ piles (see Figure 4).

Furthermore, the utilization of high-pressure slurry renders the DMJ technology more appropriate for the harder strata prevalent in the Yellow River floodplain region. The cement slurry can be more fully mixed with the soil, and the quality of pile formation is significantly enhanced, with minimal or no emergence of cement slurry. This has the additional benefit of reducing the waste of cement and other materials, as well as the environmental pollution caused by the construction process.

Figure 4. Coring of DMJ pile techniques.

The illustration below depicts the bubbling of the slurry during the formation of a DMJ pile, as observed on-site in the Yellow River floodplain. In comparison with the conventional deep mixing technique, the slurry utilized in DMJ piles is characterized by an earthy yellow hue, with the vast majority of the material comprising soil (see Figure 5).

Figure 5. Slurry bubbling of DMJ pile techniques.

2. DMJ Pile Construction Procedure

1. DMJ Variable-Modulus Piles

The cement slurry is mixed with the soil by external spraying and internal mixing. This is achieved by jetting the slurry horizontally at high pressure through the nozzle at the end of the mixing rod and by rotating the drill pipe and lifting it at low speed. The mixing rod is used to stir the return slurry and the soil, thus forming a drilling and spraying churning pile with a high-strength cylindrical wall and a low-strength cylindrical core. The formation of the pile is illustrated in Figure 6.

2. Capped DMJ Piles

The same construction method is employed for variable-modulus piles. The distinction lies in the fact that within a specific range of the pile body, a reduction in the rate of lifting is akin to the introduction of a greater volume of cement slurry into the soil layer, thereby resulting in the formation of a more robust and resilient cap with enhanced bearing capacity. This results in an enhancement of the pile body's load-carrying capacity. The formation of the pile is illustrated in Figure 7.

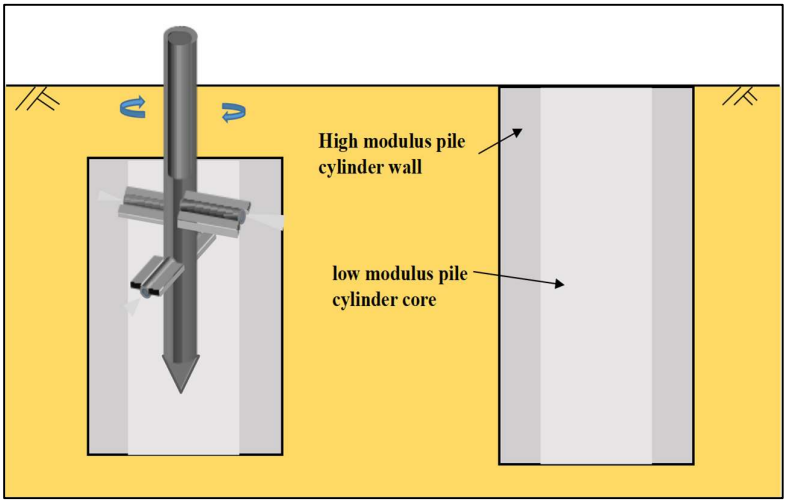

Figure 6. Schema of variable-modulus DMJ piles.

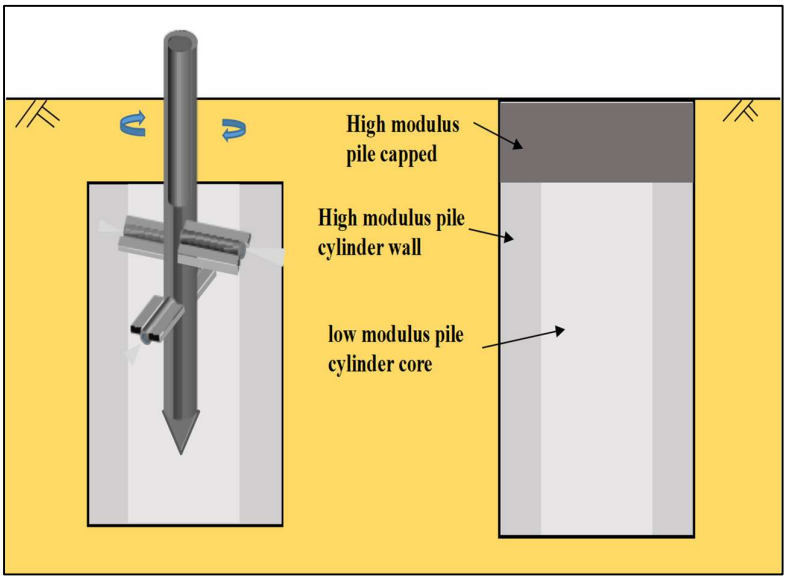

Figure 7. Schema of capped DMJ piles.

The pile types and parameters of composite foundations are still unclear, as are their bearing characteristics.

Finite element numerical simulation is the most widely used method for the numerical simulation of composite foundations. It can accurately simulate the working conditions of embankments [16,17] and is an effective approach for studying load-bearing characteristics [18]. In comparison to the intricate indoor and field tests [19], the finite element numerical method is straightforward to implement, has a low cost, and can be employed for the analysis of pile damage modes and the optimization of pile types [20]. Two-dimensional and three-dimensional finite element models have been extensively employed in the investigation of the bearing characteristics of composite foundations [21–23]. A considerable number of studies have employed the use of finite elements to develop a three-dimensional model for the analysis of the bearing characteristics of composite foundations [24–28]. Zhu et al. [29] demonstrated the load transfer behavior of a novel composite structure, namely stiffened deep cement mixing with a rigid cap in layer soils, among other examples. Jiu et al. [30] evaluate the bearing characteristics of SDCM piles under vertical loading. The excessively long cross-section of DCM piles leaves their lower part unstressed for a certain core length. In order to investigate and analyze the behavior of stiffened deep cement mixing (DCM) columns under compressive loading in loose sandy

soils, El Sawwaf et al. [31] carried out laboratory tests. The results demonstrated that reinforcement can significantly improve the load settlement response of DCM piles.

The objective of this study is to evaluate the impact of pile strength and two types of DMJ piles on single-pile bearing capacity and single-pile composite foundation bearing capacity through numerical simulation. Validation of the model was conducted through a comparison with field test results. Furthermore, the study optimizes a range of geometrical parameters associated with DMJ piles. The design calculation method for the bearing capacity of DMJ group piles under embankment loading is investigated based on the results of the field tests and numerical simulations. This paper presents a detailed discussion of the findings.

3. Numerical Simulation Modelling

3.1. Model Definition

ABAQUS finite element software was employed for the simulation of the load transfer process associated with the DMJ pile. This study used the 3D version of the ABAQUS2021 software. The simulation results are compared with the field test results in order to verify the reliability of the model and to investigate the factors affecting the load-bearing capacity of DMJ piles. The procedure for modelling a single pile is as follows:

1. Parts and Materials

A composite foundation, illustrated in Figure 8a, is constructed whereby the soil is represented by the Moore–Cullen model and the cemented soil (pile) is modelled using the linear elasticity model. In the process of modelling, the diameter of the soil body is typically set to be 20 times larger than that of the pile body, while the distance from the end of the pile to the bottom of the soil body is generally larger than 10 times the diameter of the pile body. This approach circumvents the issue of non-convergence of the calculated results and the boundary effect that can arise during numerical simulation.

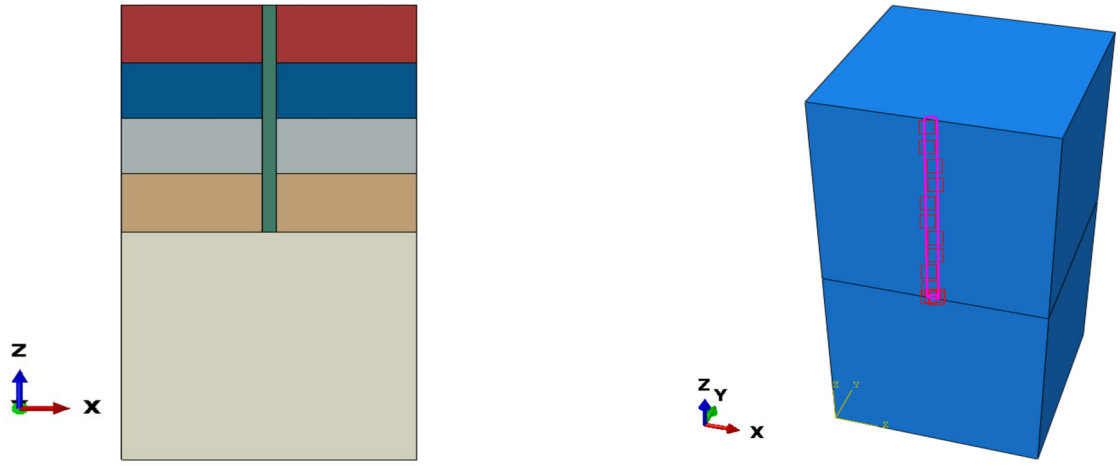

(**a**) Composite foundation modelling (**b**) Model contact settings

Figure 8. DMJ pile modelling.

2. Contact Surface

In the numerical simulation of the pile foundation, it is essential to define a suitable contact surface between the pile and the surrounding soil, as illustrated in Figure 8b. In the present study, the tangential direction of the contact surface is defined in accordance with the Coulomb shear model. The normal direction of the contact surfaces is defined as the most widely used hard contact in ABAQUS, wherein the hard contact form restricts the occurrence of penetration of the contact surfaces during the calculation process. In defining the contact pair, the face with high stiffness is designated as the primary face, while the face with relatively low stiffness is designated as the secondary face. Accordingly, the pile

is designated as the primary surface, while the soil is identified as the secondary surface, in the context of pile–soil contact.

3. Boundary Condition

The displacement of the outer edges of the soil surrounding the pile in the X and Y directions is set to zero during the establishment of the model. However, the displacements of the soil at the pile end in the X, Y, and Z directions are set to zero. In accordance with the symmetry of the pile foundation structure under vertical loading, it is sufficient to establish only half the test size of the pile-soil system for modelling and calculation purposes.

4. Grids and Iterative Algorithms

The cell types employed for model meshing are 6-plane, 8-node linear reduced integral cells (C3D8R). In this study, the default Newton–Raphson iterative method, as implemented in ABAQUS, is employed for the solution of the nonlinear system of equations.

3.2. Reliability Verification of Models

In-suit tests were conducted in accordance with the typical soil distribution observed in the Yellow River floodplain.

In order to circumvent the non-convergence of calculation results and boundary effects that may arise during the numerical simulation stage of the ABAQUS modelling process, the diameter of the soil body is typically set to be 20 times larger than that of the pile body, while the distance of the pile end from the bottom of the soil body is generally larger than 10 times the diameter of the pile body. The geometric parameters of the pile model are in accordance with those observed in the field test.

The results obtained from the numerical study are compared with the field static load test in order to verify the reliability of the developed model. In this instance, Pile 1 from Site 1 and Piles 2–6 from Site 2 were selected for comparative validation. In this study, the modulus of elasticity of the deep cement mixing piles was taken as 100 times its unconfined compressive strength, which was measured in the laboratory from samples taken on-site. The soil parameters were obtained from the field soil drilling and are presented in Table 1.

Table 1. Material parameters for single-pile modeling of DMJ piles.

Depth	**Material**	**Density (kN/m^3)**	**Plasticity Index**	**Yield Stress (kPa)**	**Internal Friction Angle (°)**	**Young's Modulus (MPa)**
			(a) Site-1			
0–5.5	Silty Clay	18.9	14.3	22.8	14.6	6.66
5.5–8	Mucky Silty Clay	18.6	17.1	32.9	8.9	4.44
8–10	Silty Clay	19.1	15.9	26.2	14.3	5.18
10–20	Silty Clay	19.2	11	23.5	15.5	7
0–10	Pile-1	21	-	-	-	700
			(b) Site-2			
Depth	Materials	Density (kN/m^3)	Plasticity Index	Yield Stress (kPa)	Internal Friction Angle (°)	Young's Modulus (MPa)
0–2	Fillings	18.7	11.8	24.5	16.6	4.13
2–6	Silt	18.8	7.7	15.5	20.5	5.36
6–10	Mucky Silty Clay	18.6	17.1	32.9	8.9	4.44
10–20	Silty Clay	19.2	11	23.5	15.5	7
0–10	Pile-2	19	-	-	-	150
0–10	Pile-3	19	-	-	-	200
0–10	Pile-4	19	-	-	-	300
0–10	Pile-5	19	-	-	-	250
0–10	Pile-6	19	-	-	-	300

Figure 9 illustrates a comparison of the load settlement behavior observed in field tests and that predicted by numerical studies. The use of numerical simulation allows for

the precise measurement of load values, whereas the actual load of the field loading test is subject to disturbance from factors such as pile head flatness. It should be noted that the load values for each level of the two curves are not identical; however, this does not impact the analysis and comparison of the data. The degree of fit (R^2) of the six sets of models to the measured data in the field was 0.93, 0.97, 0.96, 0.96, 0.98, and 0.98, respectively, indicating that the models are reliable. It is observed that the simulation method of the single pile static load test adopted in this paper can accurately reflect the results of the field test. Furthermore, it can be used for further analysis of single pile-bearing characteristics.

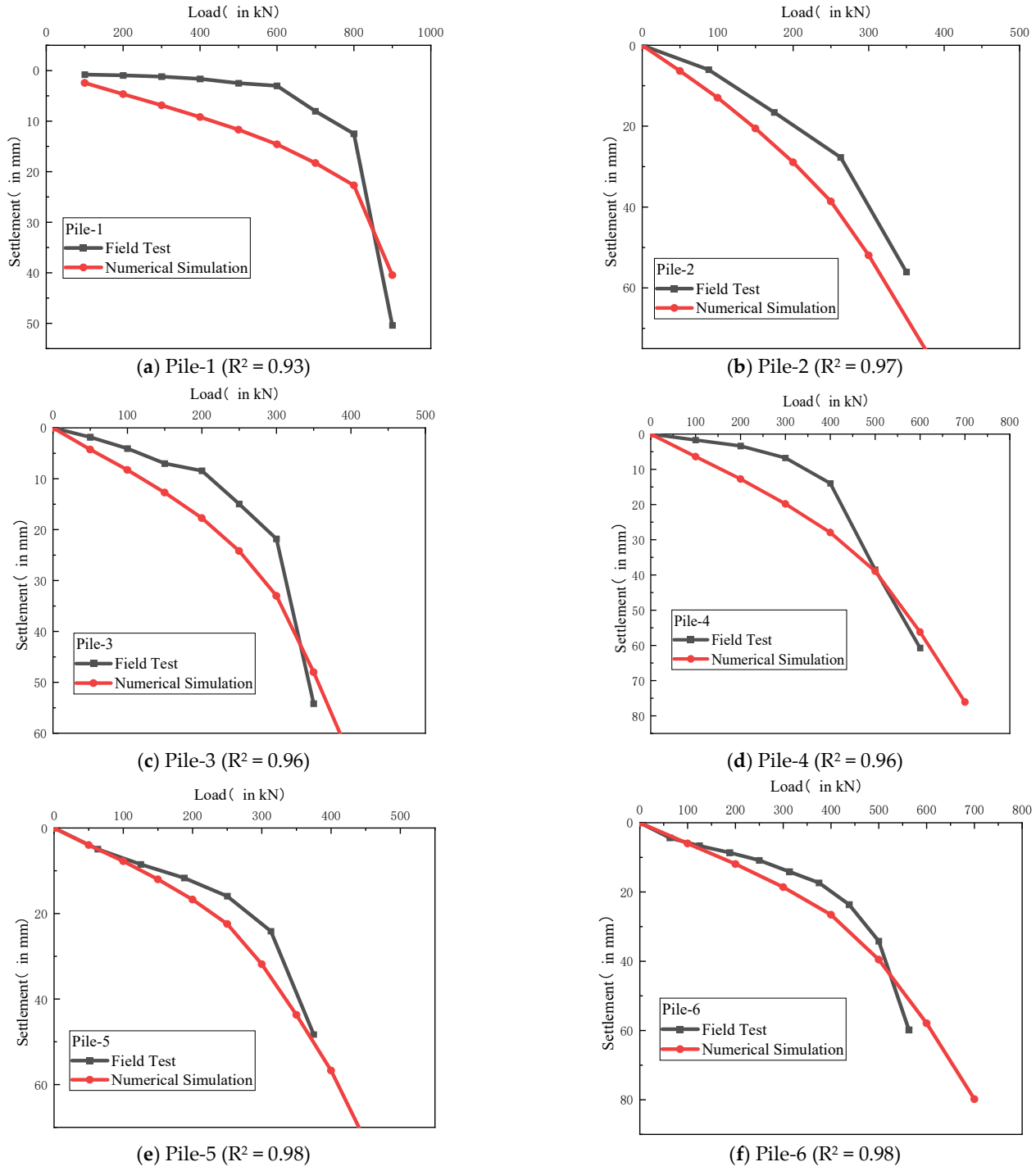

(**a**) Pile-1 (R^2 = 0.93) (**b**) Pile-2 (R^2 = 0.97)

(**c**) Pile-3 (R^2 = 0.96) (**d**) Pile-4 (R^2 = 0.96)

(**e**) Pile-5 (R^2 = 0.98) (**f**) Pile-6 (R^2 = 0.98)

Figure 9. Comparison of Q-s curves between in situ tests and numerical simulation.

4. Result and Analysis

4.1. Single Pile Bearing Characteristics of DMJ

The DMJ process is distinguished by the potential to construct piles with varying internal and external moduli, as well as the capacity to cap them by adjusting the slurry pressure and boosting speed. Accordingly, the present study focuses on the numerical simulation of a single pile, with a particular emphasis on the parameters related to internal and external moduli and capping.

For the purposes of simplicity, the foundation soil used in the numerical simulation of a monopile is represented by Yellow River floodplain silty clay. The modelling parameters are presented in Table 2. The numerical simulation scheme is presented in Table 3.

Table 2. Soil parameters for numerical simulation.

Type of Soil	Density (kN/m^3)	Plasticity Index	Yield Stress (kPa)	Internal Friction Angle (°)	Poisson's Ratio	Young's Modulus (Mpa)
Silty Clay	19	13	22.8	15	0.3	7

Table 3. Single pile static load numerical simulation conditions.

	Internal Modulus (GPa)	External Modulus (GPa)	μ		Cap Thickness (m)	Cap Modulus (GPa)	Internal Modulus (GPa)	External Modulus (GPa)	μ
M1	0.1	0.7	0.77	T1	0.5	0.7	0.1	0.35	0.69
M2	0.3	0.7	0.77						
M3	0.5	0.7	0.77	T2	1				
M4	0.7	0.7	0.77						
M5	0.1	0.2	0.56	T3	1.5				
M6	0.1	0.3	0.66						
M7	0.1	0.4	0.7	T4	2				

The objective of Cases M1 to M7 is to investigate the impact of variations in core modulus, pile-side mechanical resistance, and pile-side modulus on the bearing performance of the monopile. The modelling schematic is presented in Figure 10.

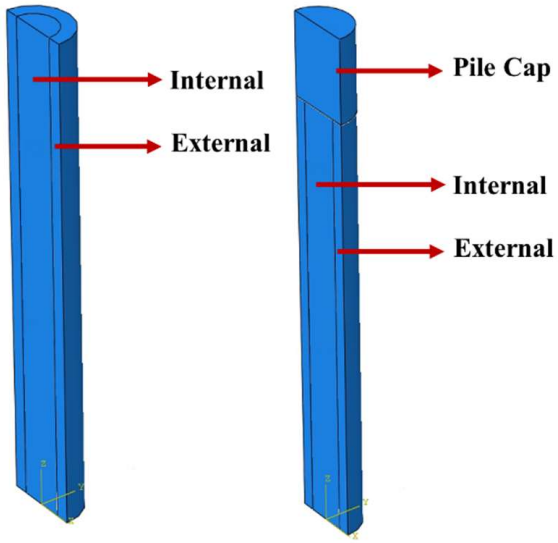

Figure 10. Schematic diagram of pile modeling.

Cases T1 to T4 are primarily concerned with examining the impact of cap thickness on the load-carrying capacity of a single pile top. In the course of the simulation, the length of each monopile is set at 10 m, while the diameter is 0.8 m. The modeling schematic is presented in Figure 10.

4.1.1. Bearing Characterization of DMJ Variable-Modulus Piles

Figure 11 illustrates the load–settlement curves of the static load simulation of DMJ piles under different scenarios. It was observed that the pile settlement increased abruptly when the applied load reached 1600 kN. The static load value corresponds to the commencement of the precipitous decline in displacement and is deemed to be the ultimate bearing capacity of the monopile. Accordingly, the ultimate bearing capacity of the single pile is determined to be 1600 kN. A reduction in the modulus of the pile core results in a larger settlement behavior prior to the attainment of the ultimate settlement. Nevertheless, the pile's outer side continues to demonstrate superior bearing capacity.

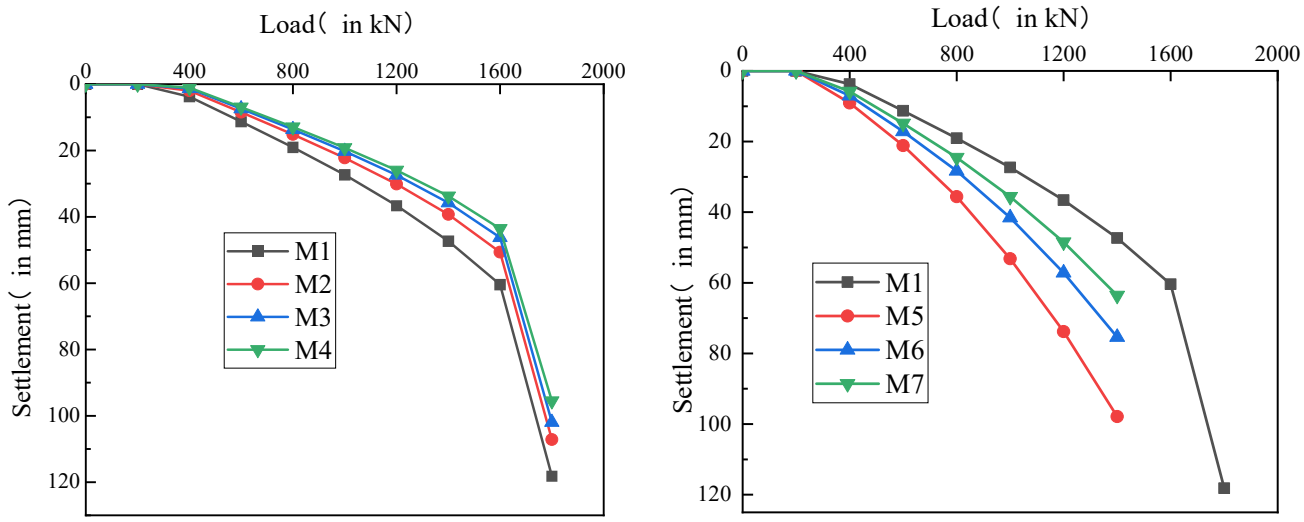

(**a**) Variable core modulus (**b**) Variable lateral modulus and friction

Figure 11. Q-s curves of single pile simulation.

The load-displacement curves for the M5 to M7 models are presented in Figure 11b. Upon reaching loads of 1000 kN, 1200 kN, and 1400 kN, damage is observed at the top of the pile, accompanied by a loss of synchronization between pile deformation and soil deformation. This can be regarded as a criterion for the damage of the pile. At this juncture, the ultimate bearing capacity of a single pile is taken to be the load value corresponding to a settlement of 40 mm, which is a commonly employed criterion for determining the bearing capacity in deep cement mixing pile projects in the Yellow River floodplain. It can thus be concluded that the ultimate bearing capacities of M5, M6, and M7 are, respectively, 850 kN, 976 kN, and 1057 kN. The ultimate bearing capacity of the pile is also affected by a reduction in material strength and pile–soil friction coefficient. A reduction in the coefficient of friction results in an increase in relative settlement between the soil and the pile, which can lead to piercing damage and ultimate failure of the pile. This will result in a reduction in the pile's bearing capacity, which may ultimately lead to the failure of the project.

A differential settlement is evident in the upper portion of the pile, resulting from the discrepancy between its internal and external modulus. Figure 12 illustrates the settlement discrepancy under varying load conditions.

It can be observed that with an increase in load, the settlement difference gradually increases. As the discrepancy between the inner and outer moduli of the pile increases, the settlement difference is observed to increase, reaching a maximum settlement difference of over 9 mm.

Further analysis of the stress distribution behavior is conducted to ascertain whether damage has occurred to the core of the pile under different loading levels and to evaluate the stress concentration in the pile body of the variable-modulus pile.

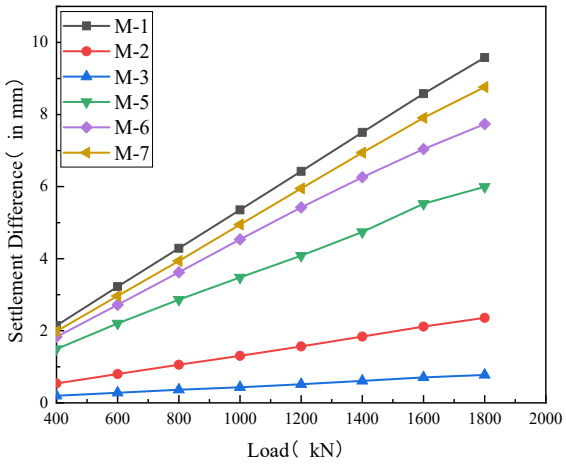

Figure 12. Settlement difference between pile core and pile outer side.

Figure 13 illustrates the stress cloud diagrams of the pile body at the ultimate load for a variety of pile types. It can be observed that the pile body stress of the variable-modulus pile is concentrated on the pile's outer side. The values displayed in the graph indicate the magnitude of the vertical stress in kPa, with a negative sign denoting the direction of the stress. A reduction in the modulus of the pile's core results in an increased stress borne by the pile's outer side, accompanied by a more pronounced stress concentration phenomenon. As the modulus of the pile core increases, the load-bearing ratio of the core also increases in accordance with the aforementioned relationship. However, the depth of the stress-concentration section on the pile's outer side decreases, thereby making the stress-concentration phenomenon less obvious. The stress of the pile body of the uniform modulus pile (M4) is concentrated at the top of the pile, with the load distributed uniformly across the top.

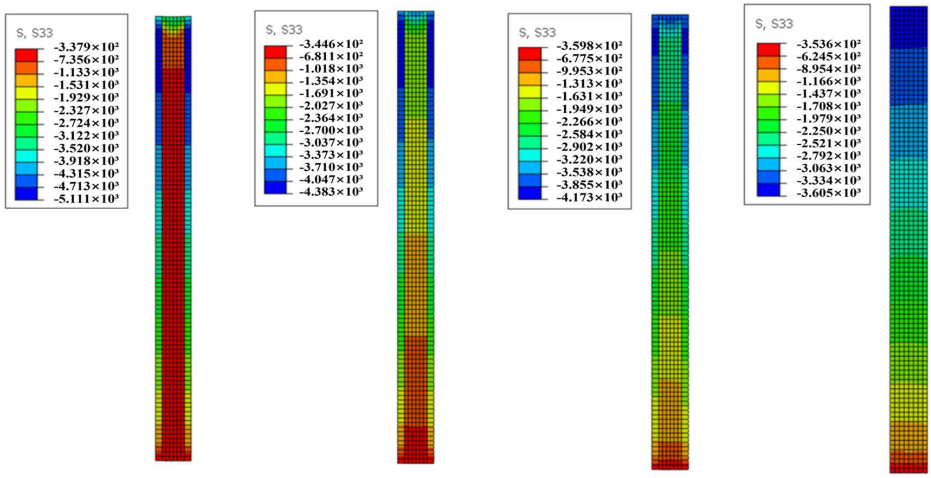

(**a**) M1 (**b**) M2 (**c**) M3 (**d**) M4

Figure 13. Stress cloud map under ultimate load with different pile core moduli.

Figure 14 illustrates the stress distribution of the core and peripheral portion of the pile for M1 to M4 conditions. From Figure 14a,b, it can be observed that the maximum value of the pile outer side stress of the variable-modulus pile M1 occurs at a depth of 0.7 m from the top of the pile, while the peak stress in the core portion of the pile is recorded at the top of the pile.

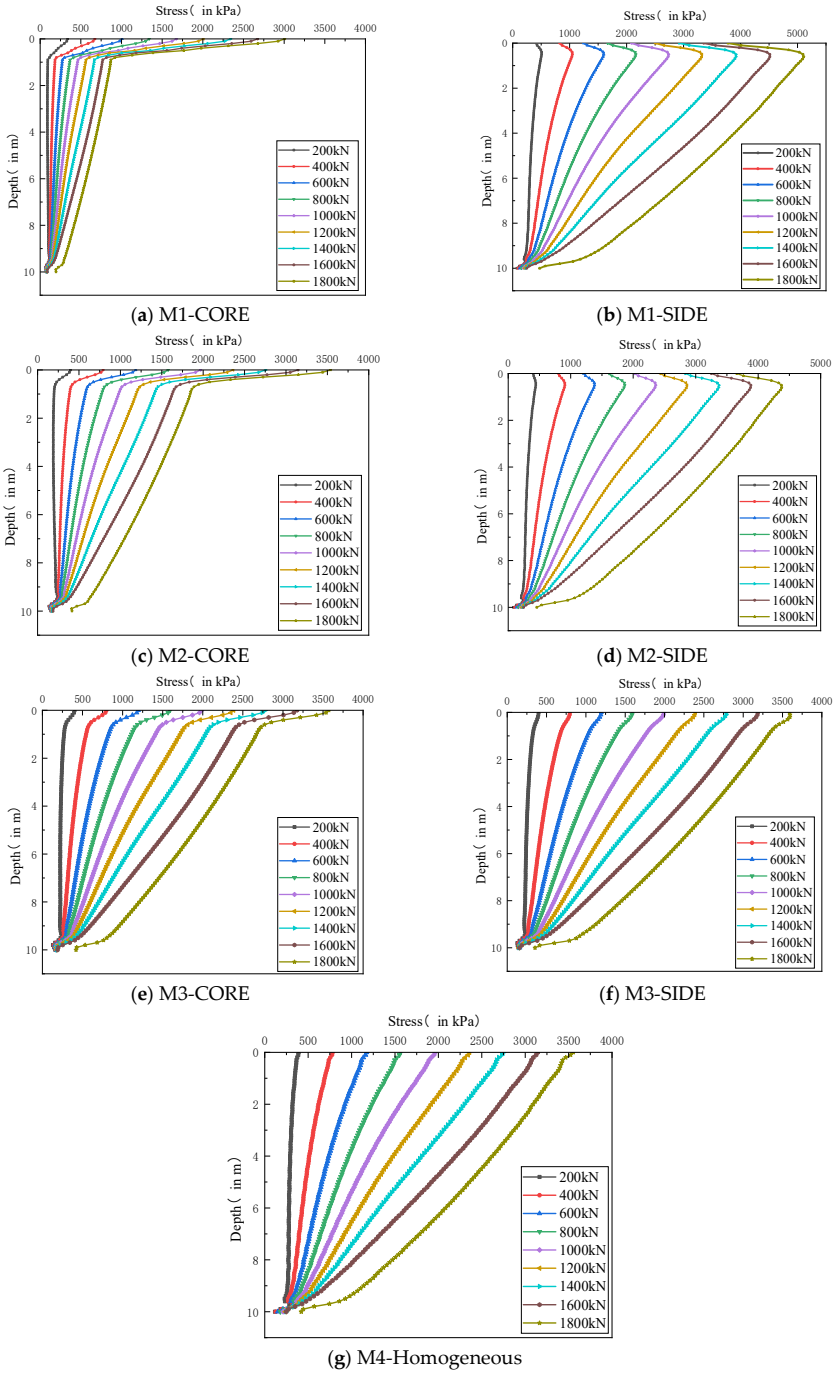

(**a**) M1-CORE (**b**) M1-SIDE

(**c**) M2-CORE (**d**) M2-SIDE

(**e**) M3-CORE (**f**) M3-SIDE

(**g**) M4-Homogeneous

Figure 14. Vertical stress distribution diagram of the piles from M1 to M4.

As can be observed from the stress distribution curve of the pile body at the pile's center, the stress at the pile's upper extremity exceeds 1000 kPa when the applied load is 600 kN. In the initial phase, the upper section of the pile experiences compression damage, while the peripheral portion has not yet reached its ultimate bearing capacity. As the load is increased gradually, the settlement difference between the pile's core and the pile's outer side also increases gradually.

As a consequence of the fact that deep cement mixing piles are typically not provided with pile caps, which can give rise to a number of issues, including damage occurring at an early stage and the uneven settlement of the pile top in actual road projects, it is necessary to reinforce the strength of the pile core's material.

Figure 14c,d demonstrate that the pile stress distribution pattern of the variable-modulus pile M2 is analogous to that of M1.

The stress on the pile core's upper surface exceeds 3000 kPa when a load of 1600 kN is applied, exceeding the ultimate bearing capacity. It can thus be inferred that the modulus of the pile core must be 0.3 GPa in order to satisfy the ultimate state of the pile body under pressure.

Figure 14e,f illustrate the vertical stress curves when the modulus of the pile core is increased to 0.5 GPa. At this juncture, the stress concentration phenomenon on the pile's outer side is not significant; however, the pile core reaches its limit value of bearing capacity.

The stress in the upper position of the pile core exhibits comparable magnitudes under disparate conditions. It is essential to ensure that the top portion of the pile is sufficiently robust in terms of material strength. The rate of reduction in pile core stress is observed to decrease with depth, as the pile center modulus increases.

The application of a load with a magnitude of 1800 kN resulted in a significant reduction in stress at a depth range between 0 and 0.7 m of pile M1's core, from 3500 kPa to 800 kPa.

In contrast, for M2, the stress reduction is from 3500 kPa to 2000 kPa as the depth of the pile changes from 0 to 0.7 m. For M3, the reduction is from 3500 kPa to 2700 kPa. It is noteworthy that in the case of M4, the pile stress exhibits a uniform decrease with depth.

As illustrated in Figure 14, the stress distribution curve demonstrates that maintaining a constant modulus at the pile's center while reducing the modulus at its outer edge results in a decline in the pile's ultimate load-carrying capacity. This is due to a simultaneous reduction in the strength of the pile and the pile-soil friction coefficient, which, when considered together, results in a decrease in the pile's bearing capacity.

Figure 15 illustrates the extracted vertical stress clouds of the profiles of the pile's outer side when damaged from M5 to M7. The values displayed in the graph indicate the magnitude of the vertical stress in kilopascals (kPa), with a negative sign denoting the direction of the stress. Upon reaching the ultimate bearing capacity of the material, the outer side of the pile experiences a failure in advance of the ultimate load, resulting in damage to the pile body. This suggests that if the pile's outer side is not capable of withstanding its ultimate load, early damage will occur and capping will be required to protect the pile head.

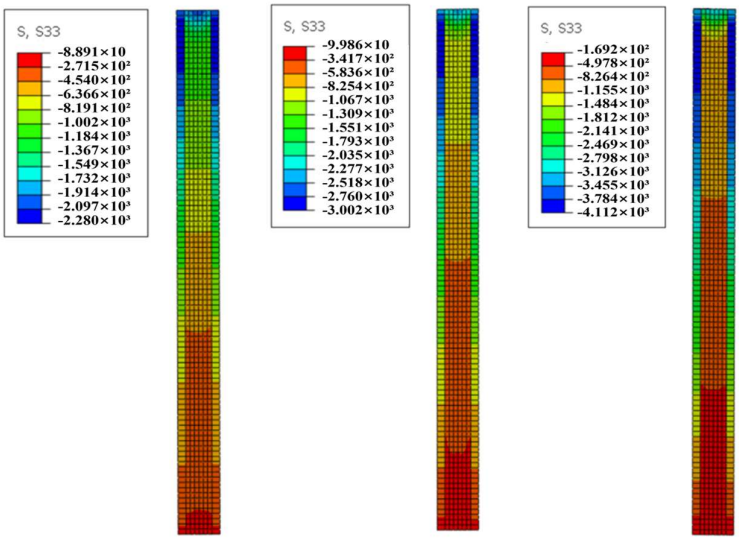

(**a**) M5 (**b**) M6 (**c**) M7

Figure 15. Stress cloud map of the piles from M5 to M7.

4.1.2. Bearing Characterization of Capped DMJ Piles

To address the issue of premature pile top failure, simulations of capped piles T1 to T4 were carried out based on existing DMJ technology. In actual construction, the top of the pile is constructed slowly to increase the cement dosage to form a high-strength solid cap, and the bottom of the pile is constructed quickly to control the cement dosage to form a tubular pile. In this study, both the modulus of the cap and the modulus of the tubular pile are obtained from the results of field tests.

The load–settlement curves of individual piles were extracted, as shown in Figure 16. T1 piles were damaged at the pile head under a load of 1080 kN to stop loading, T2 and T3 piles were damaged at the pile head under a load of 1400 kN, and T4 piles were damaged at the pile head under a load of 1600 kN.

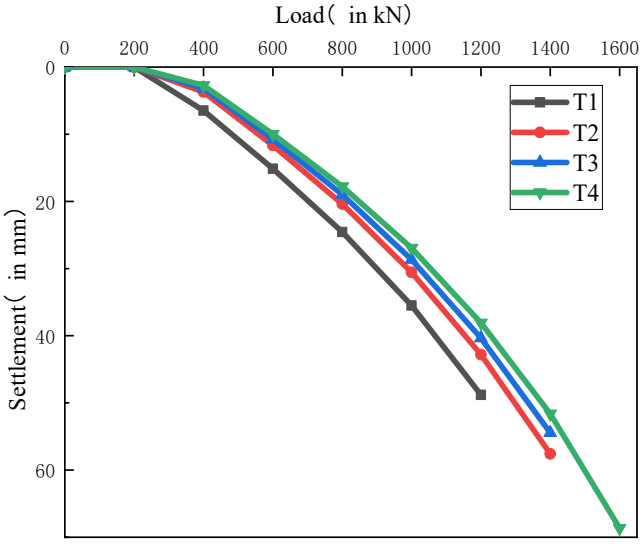

Figure 16. Load–displacement curve of capped pile.

Prior to pile damage, a minimal change in the load-displacement curves was observed, so the load value corresponding to the 40 mm settlement value was taken as the ultimate capacity of a single pile. The ultimate bearing capacity of a single pile for T1 was 1080 kN and the ultimate bearing capacity of a single pile for T2 was 1150 kN, which was 11.5% higher than that of T1, and the ultimate bearing capacity of a single pile for T3 and T4 was 1196 kN and 1235 kN, which were 4% and 7.4% higher than that of T2.

This illustrates a minimal increase in bearing capacity. The capped pile avoids early damage because the top of the pile carries most of the load, the cement content of the top of the pile is higher, and its coefficient of friction is also higher, which is more conducive to synergistic deformation of the pile-soil at the top of the pile.

The applied vertical stress is removed when the ultimate strength of the material is reached, as shown in Figure 17. The values in the graph indicate the magnitude of the vertical stress in kPa and the negative sign indicates the direction of the stress. If the cap thickness is 0.5 m, the stress will be concentrated in the range of 0.5–1 m at the top of the pile. At this time, it will aggravate the stress concentration of the pile's outer side material, and the pile's outer side will be damaged in advance when the overlying load reaches 1000 kN, as illustrated in Figure 17a.

After the thickness of the capping is increased to 1 m, the stress concentration on the outer side of the pile is relieved. At this time, the load can be transferred more evenly to the lower pile body and the grade of the pile's outer side material that can bear the load increases from 1000 kN to 1400 kN, as illustrated in Figure 17b.

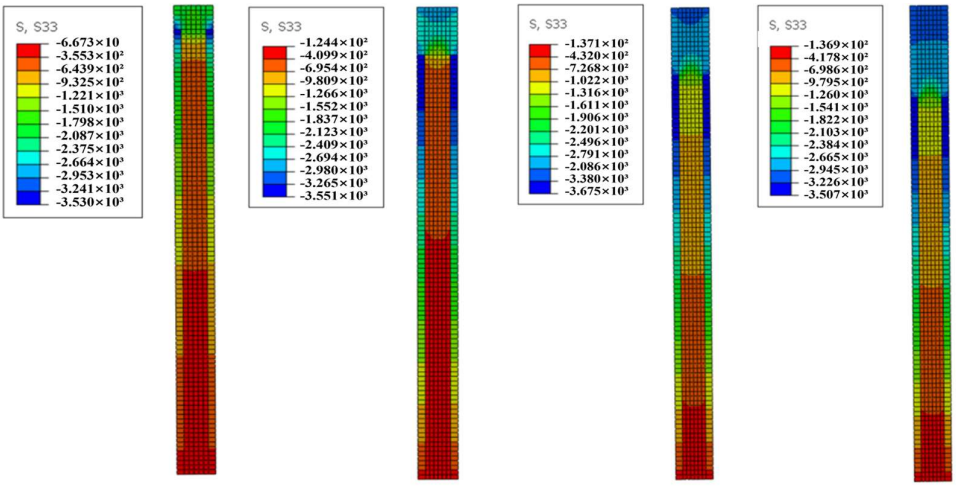

(**a**) T1 (**b**) T2 (**c**) T3 (**d**) T4

Figure 17. Vertical stress cloud map of capped pile.

After the capping thickness continues to increase to 1.5 m and 2 m, the stress concentration phenomenon on the pile's outer side is further relieved, and the grade of the pile's outer side material that can bear the load when it is destroyed is increased to 1600 kN, but it does not have a big increase compared with that of the 1 m capping, as illustrated in Figure 17c,d.

It can be seen from the vertical stress distribution diagram that the stress concentration phenomenon on the pile body becomes more pronounced as the thickness of the cap decreases.

The locations of stress concentration all appeared at the junction of the capping and variable-modulus cylinder pile, and the difference in strength between the pile's outer side and the pile's core resulted in the sudden change in stress concentration.

As shown in Figure 18a,b, when the capping is 0.5 m thick, the top of the pile carries a greater proportion of the load due to its higher strength. Its maximum pile stress occurs at the sudden change in the pile outer side's modulus, where the change in modulus brings about a sharp increase in pile outer side stress. The outer side stress of the pile reaches 3500 kPa in the process of the load increasing from 800 kN to 1000 kN, which exceeds the ultimate strength of the pile's outer side, and the maximum stress on the pile's outer side is 6246 kPa when the overlying load is 1800 kN.

As shown in Figure 18c,d, the sudden change in stress improved significantly after the cap thickness was increased to 1 m. The pile's side stress reaches the ultimate value of pile strength when the upper load is 1400 kN, and the maximum stress on the pile's outer side decreases to 4400 kPa by continuing to increase the load to 1800 kN, which is 29.5% less than the ultimate stress on the pile's outer side at the capping thickness of 0.5 m.

When the capping thickness continued to increase, the extreme values of stress concentration on the outer side of the pile were reduced to 4250 kPa and 4085 kPa, which were 3.4% and 7.2% less than that of the capping at 1 m thickness, and the magnitude of the reduction was smaller.

At a 0.5 m capping thickness, the pile core's stress at 0.6 m depth reaches 1138 kPa when loaded with 600 kN, which exceeds the ultimate strength.

When the cap thickness is increased to 1 m and 1200 kN is applied, the pile core's stress at 1.1 m depth is 1010 kPa, which reaches the ultimate strength. It can be said that the pile core will not be damaged before reaching the ultimate load limit.

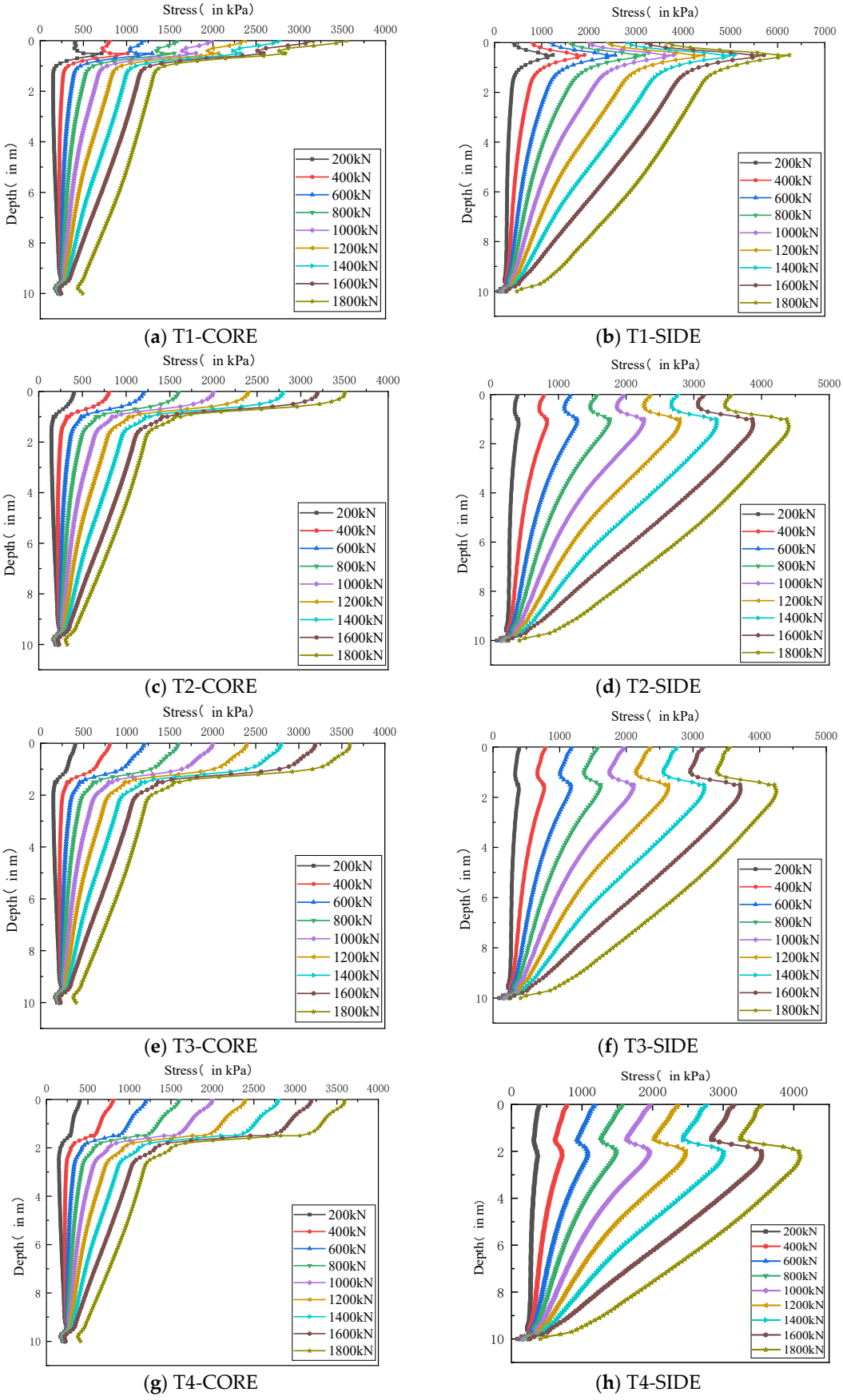

(**a**) T1-CORE (**b**) T1-SIDE

(**c**) T2-CORE (**d**) T2-SIDE

(**e**) T3-CORE (**f**) T3-SIDE

(**g**) T4-CORE (**h**) T4-SIDE

Figure 18. Vertical stress distribution diagram of piles T1 to T4.

After increasing the capping thickness to 1.5 m and 2 m, the stress in the pile core is smaller and the pile core will not be destroyed in advance.

In summary, the capping treatment can prevent premature damage to the pile core at the top of the pile. This is conducive to improving the bearing capacity of a single pile, and the stress concentration phenomenon at the junction of the capping and the pile's outer side is obviously relieved; thus, the 1 m capping treatment is a more suitable method of pile top treatment.

4.2. Bearing Characterization of Composite Foundations with DMJ Piles

The simulation scheme is presented in Table 4 below for reference. The experimental setup comprises five distinct groups: F1, a low-strength conventional soil mixing pile serving as a control group; F2, a DMJ pile exhibiting uniform modulus; F3 and F4, DMJ piles with variable moduli; and F5, a simulation of DMJ piles with an upper cap at 1 m.

Table 4. Static load numerical simulation of single-pile composite foundation.

	Diameter/m	Internal Modulus (GPa)	External Modulus (GPa)	Loading Method
F1	0.5	0.2	0.2	Control pile spacing of 1.2, 1.5, 1.8, 2.1 m, applying pressure on the top of the bearing plate
F2	0.8	0.7	0.7	
F3	0.8	0.1	0.7	
F4	0.8	0.3	0.7	
F5	0.8	0.1	0.35 (Cap:1 m)	

The diameters of the overlying load plates in the simulation were employed as the equivalent circular diameters of the loads distributed among a single pile at varying pile spacings.

In this simulation, the most commonly used method of arranging deep cement mixing pile composite foundations in the Yellow River floodplain is employed, namely, the equivalent circular diameter conversion method of equal triangularly arranged piles. This method is based on the relationship d = 1.05 s, where d is the equivalent circular diameter of the treated foundation area shared by a single pile and s is the pile spacing.

4.2.1. Bearing Capacity of Composite Foundations

It has been established that the cumulative settlement of the load-bearing plate should exceed 6% of its width or diameter, which serves as the criterion for the limitation of loading. In accordance with the varying dimensions of the bearing plates, the maximum permissible settlement values are 75.6 mm, 94.5 mm, 113.4 mm, and 132.3 mm, respectively.

Figure 19a illustrates the load settlement curves of F1 prior to the cessation of loading for varying pile spacings. It can be observed that the curves exhibit a comparatively gradual variation. The load value corresponding to a settlement value of 0.008 times the diameter of the bearing plate is taken as the characteristic value of the bearing capacity of the single-pile composite foundation.

As the pile spacing increases from 1.2 m to 2.1 m at increments of 0.3 m, the characteristic value of the single-pile composite foundation's bearing capacity is observed to decrease. The values are 250 kPa, 190 kPa, 184 kPa, and 163 kPa, respectively.

Figure 19b illustrates the load–settlement curve of F2. It is evident that an increase in pile diameter and strength will lead to a notable enhancement in the composite foundation's bearing capacity. Additionally, the impact of pile spacing on the strength behavior of the composite foundation is pronounced when the spacing is minimal.

It can be observed that each curve exhibits a discernible ultimate load and scale limit. Furthermore, it can be discerned that the characteristic value of composite foundation-bearing capacity diminishes in a gradual manner with the increase in pile spacing. The characteristic values of composite foundation bearing capacity are 700 kPa, 450 kPa, 350 kPa, and 300 kPa, respectively.

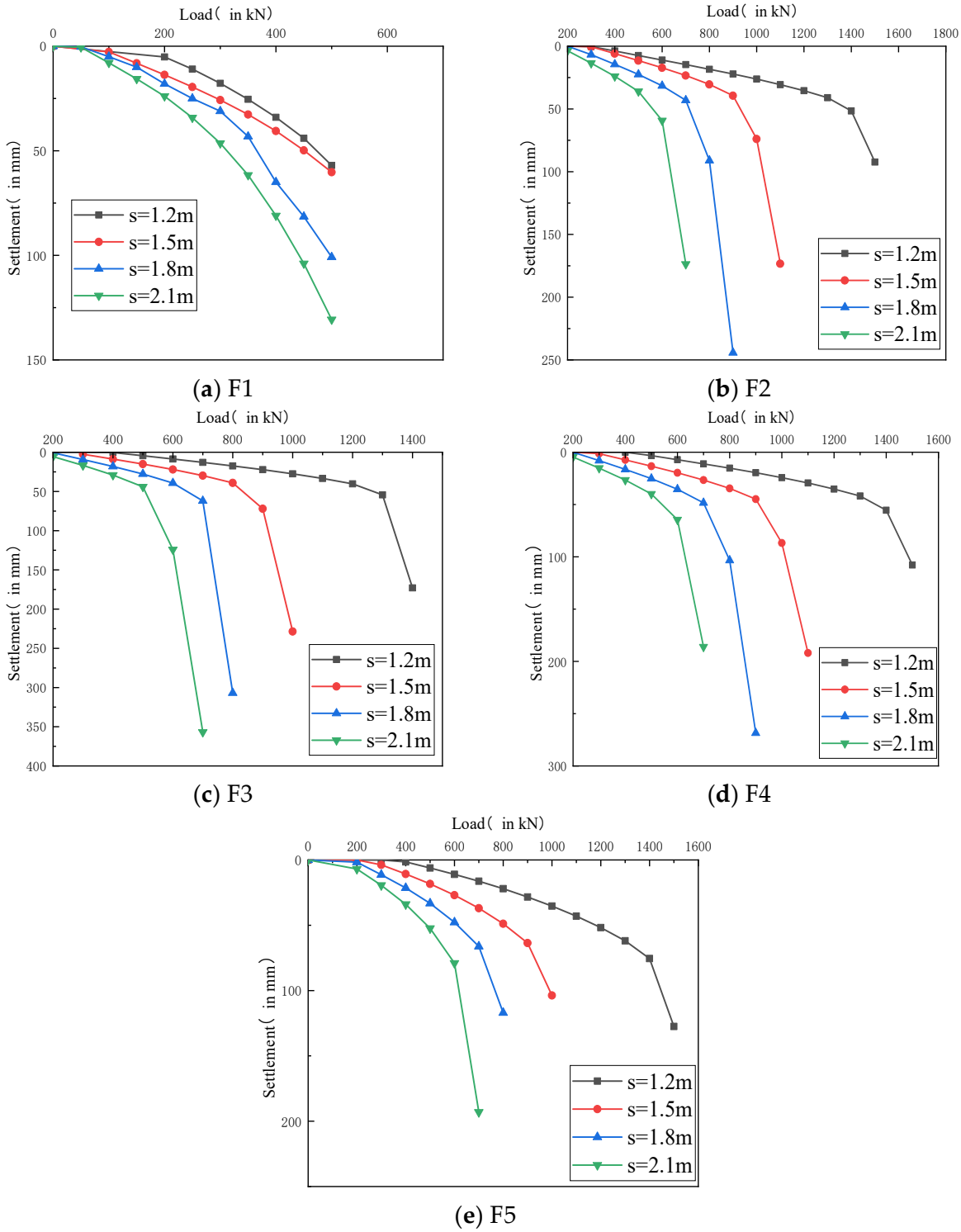

Figure 19. Q-s curves of piles with different cap lengths.

Figure 19c,d illustrate the load-displacement curves of F3 and F4 under varying pile spacings, demonstrating that the distinction in pile core modulus exerts a discernible impact on the composite foundation's bearing capacity.

A reduction in the modulus of the pile's core will result in a corresponding decrease in the characteristic value of the composite foundation's bearing capacity. A reduction in the pile core's modulus will result in a decline in the pile's bearing capacity. However, a gradual decrease in composite foundation-bearing capacity is observed. This may be

attributed to the fact that the load is not directly acting on the pile top, but rather transferred to the pile top and the soil surrounding the pile through the bearing plate.

This serves to mitigate the impact of the disparity in pile modulus on the bearing capacity to a certain extent, thereby enhancing the utilization of the synergistic effect between pile and soil.

Given the pile spacings of 1.2 m, 1.5 m, 1.8 m, and 2.1 m, the characteristic bearing capacity values for the F3 composite foundation are 650 kPa, 400 kPa, 350 kPa, and 250 kPa, respectively. The corresponding values for the F44 composite foundation are 700 kPa, 450 kPa, 350 kPa, and 300 kPa.

Figure 19e illustrates the load-displacement curve for F5. It is evident that following the application of an upper capping, the composite foundation's bearing capacity exhibits an enhancement in comparison to that observed for F3. This value is found to be identical to that of the composite foundation bearing capacity's eigenvalue of a solid pile in the F2 condition. As the pile spacing increases, the composite foundation bearing capacity's eigenvalues of F5 are observed to be 700 kPa, 450 kPa, 350 kPa, and 300 kPa, respectively.

4.2.2. Pile–Soil Stress Distribution

The distribution of stress in piles of soil under different spacing conditions exhibits a similar pattern. For the purposes of this analysis, the working condition of a 1.2 m pile spacing has been selected. Figure 20a illustrates the vertical stress distribution of the soil in proximity to the pile in F1. As the load is increased, the stress of the soil on the side of the pile reaches a maximum at the point of contact with the pressure plate, after which it decreases gradually. A minimum stress value is recorded at a distance between 1 and 2 m from the top of the pile.

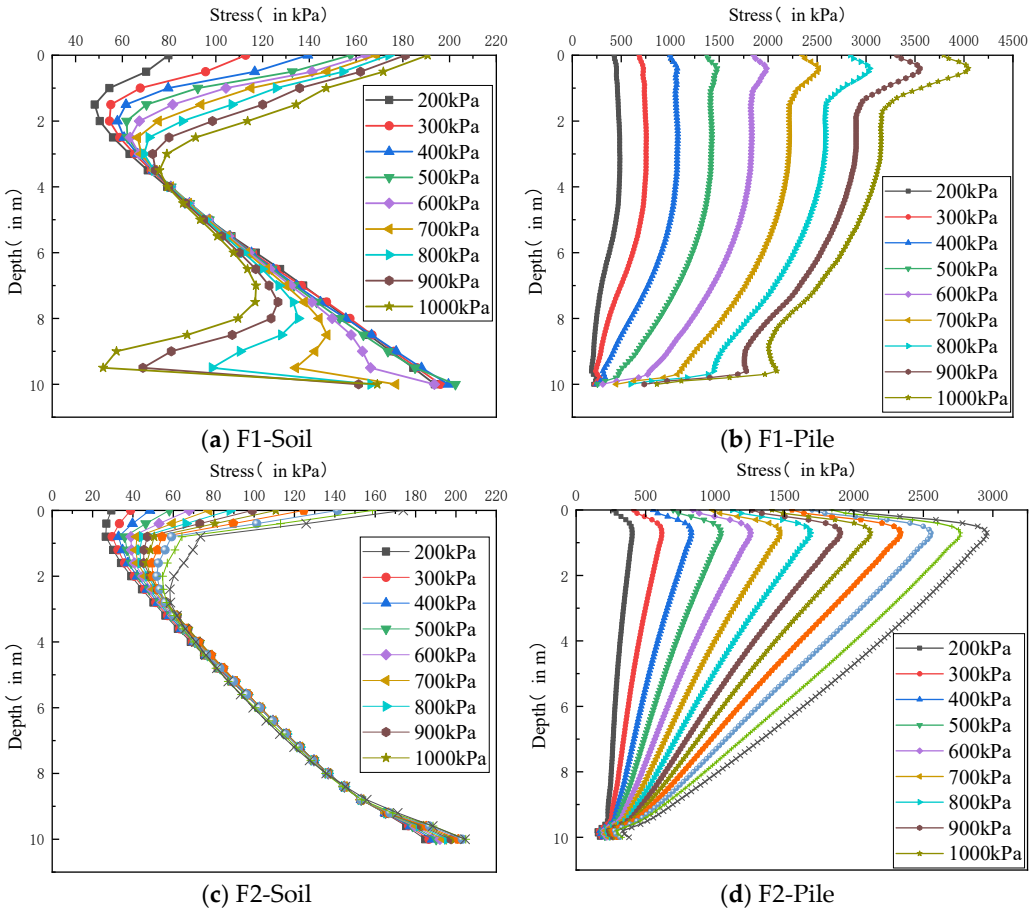

Figure 20. Vertical stress distribution diagrams of soils and pile body of piles F1 and F2.

Upon the application of an additional load of 600 kPa, a notable decline in stress was observed in the soil adjacent to the pile, with a corresponding reduction in depth. The depth at which the stress reduction occurs decreases as the magnitude of the overlying load increases. At an overlying load of 700 kPa, the depth at which the stress begins to decrease is 8.5 m from the top of the pile. At an overlying load of 1000 kPa, the location at which the stress begins to decrease is 7.5 m from the top of the pile.

This phenomenon can be attributed to the pile-piercing damage caused by the excessive load, which results in an expansion of the plastic zone at the bottom of the pile and a subsequent decrease in soil stress. However, at a distance of 9.5–10 m from the pile top, the soil stress appears to increase once more due to the vertical compression of the pile.

As illustrated in Figure 20b, the distribution of stress within the pile body reveals a peak value occurring at a depth range between 0 and 1 m from the pile top. However, beyond this depth range, the magnitude of the stress in the pile body decreases gradually. At a depth of 0–2 m from the top of the pile, the stress within the pile body is significantly greater than that within the soil. This represents the point at which the stress within the pile body reaches its maximum value, while the stress within the soil reaches its minimum value. As the load is gradually transferred to the deeper part of the pile, the stress in the pile body in this region also demonstrates a tendency to slow down the rate of load reduction. This is in line with the observed reduction in soil stress on the outer side of the pile.

Figure 20c illustrates the stress distribution of the soil in proximity to the F2 pile. The stress in the soil at the pile's outer side reaches a maximum at 0–1 m, subsequently decreasing to a minimum at 1–2 m, and then increasing slowly until reaching another peak at the pile end.

The stress in the soil at the pile end for the pile with a diameter of 0.8 m is slightly smaller than the stress value at the pile with a diameter of 0.5 m. This discrepancy may be attributed to the larger contact surface area between the pile and soil as the diameter of the pile increases. This resulted in an increase in frictional resistance at the contact surface, which in turn led to a reduction in the percentage of pile end bearing.

The pile stresses are illustrated in Figure 20d. As the pile diameter increases, the loaded area of the 0.8 m pile diameter is observed to be 2.56 times that of the 0.5 m pile diameter. Additionally, the stress within the pile body is observed to decrease significantly, with a uniform reduction in stress from the pile's upper portion to its base. This configuration thus ensures the higher bearing capacity of the large-diameter DMJ piles.

The stress distributions in the variable modulus region at the pile centers of variable-modulus piles F3 and F4 are illustrated in Figure 21a,c respectively. From these figures, it can be observed that the pile center of F4 is capable of bearing greater stress, which is approximately two times the stress borne by the pile center of F3. This is due to the difference in the modulus of the pile cores.

In the load range of 200 kPa to 500 kPa, the stresses at the pile core demonstrate a gradual increase with depth. This is due to the fact that when the load is relatively low, the stress concentration on the pile's outer side is not readily apparent. At this point, the entire pile body undergoes integral deformation, with the pile core's bearing capacity being fully utilized. Consequently, the stress within the pile core increases with depth.

Upon exceeding a load of 600 kPa, the proportion of the pile's outer side bearing the load increases. The stress in the pile core demonstrates that the stress in the upper portion of the pile initially rises and then declines gradually below a depth of 1 m. The modulus of the pile core, which is 0.1 GPa, results in a pronounced reduction in stress in the central portion of the pile within the range of 9.5 m to 10 m, reaching a value of 600 kPa. This is due to the fact that the modulus in the center of the pile is relatively low, and the concentration of stress on the outer side of the pile is also more pronounced. The majority of the stress is borne by the pile's outer side with a large modulus when transferred to the deep part. The proportion borne by the pile's core is minimal, and at the pile's end, the pile's core is almost not involved in load-bearing. Consequently, the stress in the pile's core rapidly reduces at the end of the pile.

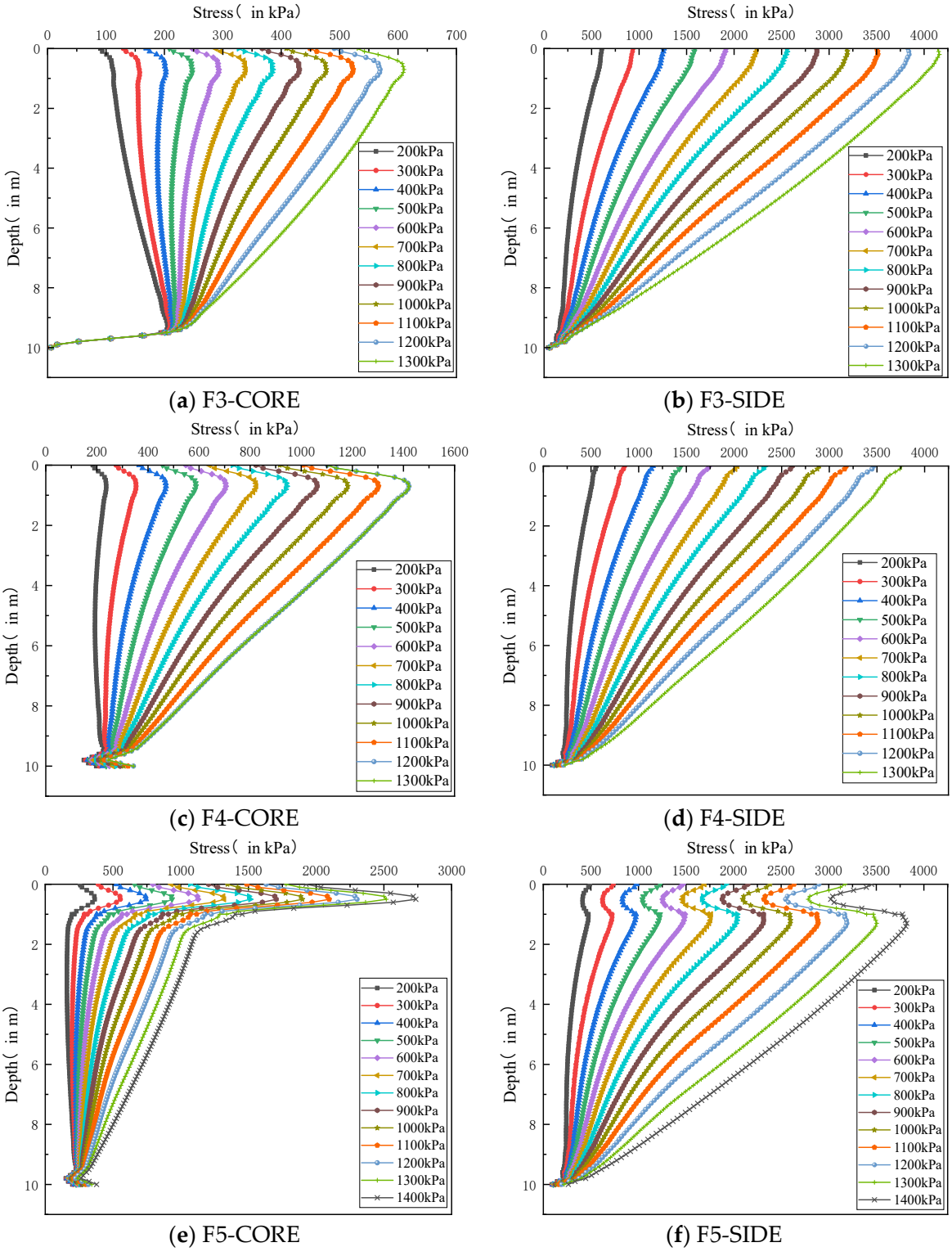

Figure 21. Vertical stress distribution diagrams of pile outer side and core from F3 to F5.

The stress distributions of the F3 and F4 piles' outer sides are illustrated in Figure 21b,d, respectively. It can be observed that the outer-side stresses in both cases decrease in a linear fashion with depth. The peak stresses on the outer side of pile F4 are smaller, which can be attributed to the fact that the higher-strength pile core bears a larger proportion of the load.

4.2.3. Differential Settlement of Piles and Soil

The present study compares and analyzes the differences in the pile and surrounding soil settlement under various working conditions to investigate the phenomenon of pile–soil differential settlement under overlying homogeneous loading conditions.

It is established that an increase in the magnitude of the load results in an increase in the differential settlement between piles and soil. It was observed that an increase in pile spacing resulted in a notable differential settlement between the pile and soil.

A comparison between conventional mixing piles with a 0.5 m pile diameter and DMJ piles with a 0.8 m diameter is presented in Figure 22a,b, respectively. It was observed that the pile with the larger diameter exhibited the least differential settlement of pile and soil, which is regarded as an optimal condition for the synergistic deformation of pile and soil.

In the F1 case, the pile-soil differential settlement increases in a linear fashion with the increase in load. The differential settlement between soil and pile is observed to increase in conjunction with an enlargement in the pile spacing. At a pile spacing of 2.1 m, the pile–soil differential settlement reaches 16 mm at a load of 100 kPa, and thus it is no longer included in the comparison curve.

In the case of F2, the differential settlement between the piles and the surrounding soil is less than 1 mm at a pile spacing of 1.2 m, which is almost negligible. For pile spacings of 1.5 m and 1.8 m, the pile–soil differential settlement increases at a gradual rate in conjunction with the rise in load. A sudden increase in differential settlement is observed when the pile spacing is 2.1 m. Following an exceedance of 800 kPa, a notable reduction in differential settlement is observed due to the joint destruction of pile and soil. However, the data for pile–soil differential settlement are not extracted beyond 900 kPa, due to the interruption of the modelling calculation caused by the excessive settlement of the pile.

The pile–soil differential settlements of variable-modulus piles are illustrated in Figure 22c,d. At both 1.2 m and 1.5 m pile spacings, a minimal differential settlement between pile and soil is observed, with a value of less than 1 mm. Upon increasing the pile spacing to 1.8 m, the differential settlement of F3 initially rises before declining and remaining constant when the applied load surpasses 800 kPa. This is due to the fact that the ultimate bearing capacity of the composite foundation has been exceeded at this point in time, resulting in the failure of the piles and the deformation of the pile and soil in a synergistic manner under the influence of the load plate.

A reduction in the settlement difference is observed when the pile spacing is 2.1 m, irrespective of the prevailing conditions. It can be reasonably deduced that the application of 800 kPa and 900 kPa has exceeded the limit value of the composite foundation bearing capacity. An additional increase in load will result in the failure of the pile body, leading to the simultaneous destruction of the pile and soil. During this phase, the differential settlement will undergo a corresponding alteration.

Figure 22e illustrates the pile–soil differential settlement of the variable-modulus piles capped at zero depth. It was observed that for a pile spacing of 1.2 m, the settlement difference was less than 1 mm. Upon increasing the pile spacing to 1.5 m, a linear increase in the settlement difference was observed, with values ranging between 0.5 and 1.5 mm. When the pile spacing was 1.8 m, the settlement difference increased from 0.69 mm to 4.3 mm approximately linearly before the 900 kN load, and then the increase in settlement decreased due to the ultimate load being reached. When the pile spacing is 2.1 m, the settlement difference increases in a linear fashion before reaching an inflection point at 800 kPa, after which it increases slowly. Upon reaching the ultimate load, a stable differential settlement is observed. However, when the load continues to increase, the pile body is destroyed, resulting in a loss of bearing capacity. Consequently, the pile–soil differential settlement decreases.

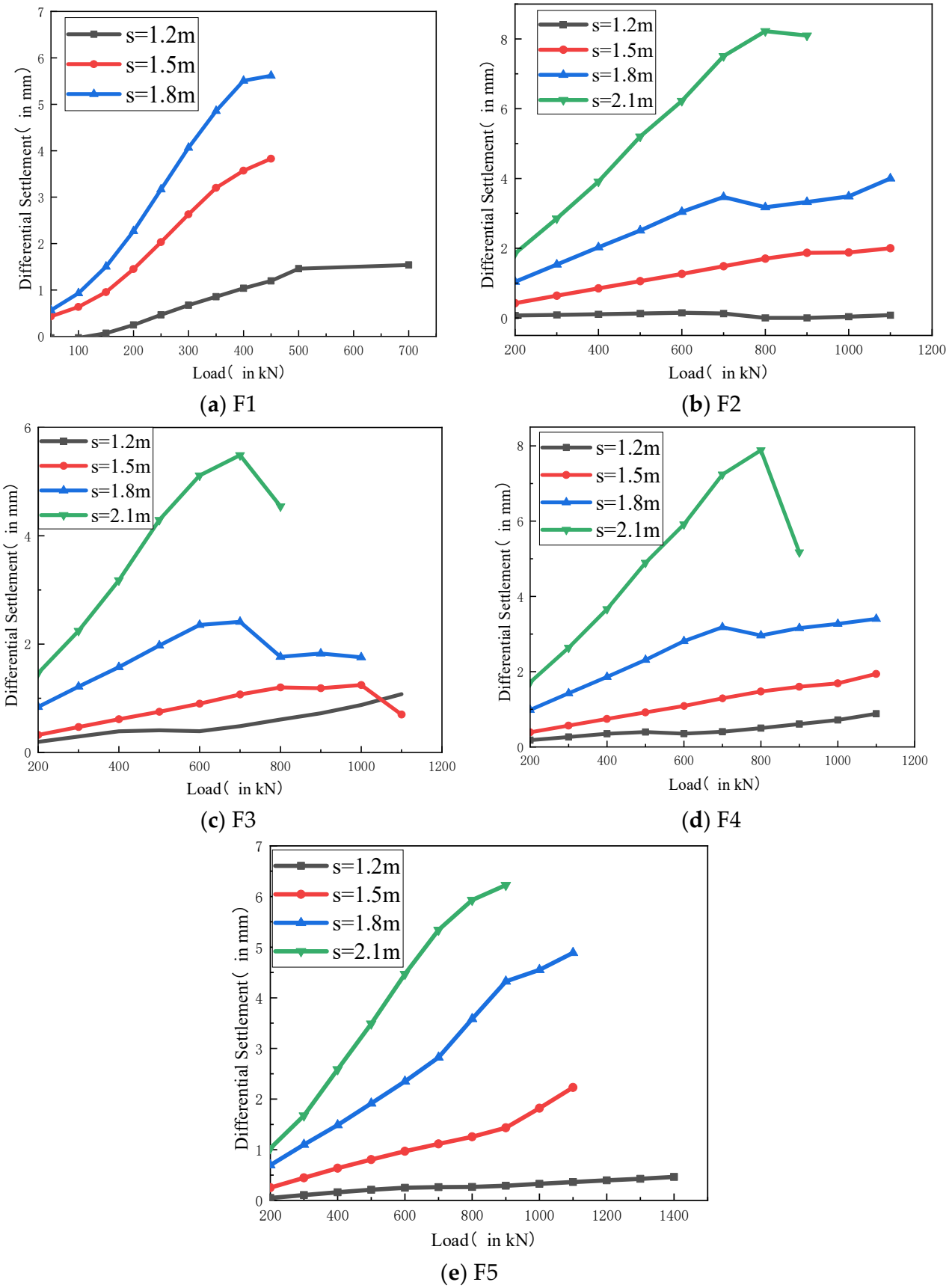

Figure 22. Pile–soil differential settlement of pile from F1 to F5.

The analysis indicates that an increase in the diameter of DMJ piles can significantly enhance the bearing capacity of the composite foundation and reduce the pile–soil differential settlement. Furthermore, it was observed that an increase in pile spacing was also prone to pile–soil differential settlement in the vicinity of the ultimate load.

5. Conclusions

This study presents a numerical simulation of the DMJ pile and investigates its bearing characteristics to optimize the DMJ pile process. Based on the investigation, the following conclusions are drawn;

1. The larger the strength difference between the inner and outer sides of the variable-modulus drilled pile, the more pronounced the stress concentration phenomenon became. The maximum stress of the single pile generally occurs at a depth of 1 m from the top of the pile.
2. It can be concluded that a DMJ pile with variable core moduli will not affect the ultimate bearing capacity of a single pile. However, the upper part of the pile and the side wall of the pile will be damaged prematurely due to insufficient bearing capacity and stress concentration.
3. It is recommended that the modulus of the pile core should reach at least 0.3 GPa or be capped after 1 m or more to avoid early destruction during the bearing process of a single pile. It can be observed that an increase in pile diameter and an elevation in pile body modulus will result in a proportional enhancement of the bearing capacity of the single-pile composite foundation. The utilization of large-diameter DMJ piles has been demonstrated to markedly enhance the bearing capacity of composite foundations, whilst concurrently reducing the extent of pile–soil differential settlement.
4. Pile spacing represents a pivotal parameter, with an increase in the aforementioned parameter resulting in an undesirable and excessive pile–soil differential settlement.
5. DMJ piles can effectively enhance bearing capacity, although their upper portions are susceptible to damage. In accordance with the specifications of the project, a capping treatment may be incorporated as required.

Author Contributions: Methodology, Y.W. and Z.S.; software, Y.W. and K.Z.; validation, Y.Z., Y.W. and Y.Z.; formal analysis, K.Y., Z.Y. and Y.R.; investigation, Y.W. and R.X.; resources, Y.Z. and Z.S.; data curation, Y.Z. and Z.S.; writing—original draft preparation, W.F.; writing—review and editing, K.Y. and Z.Y.; visualization, J.L.; supervision, J.L. and Z.S.; project administration, K.Y. and Z.Y.; funding acquisition, Y.Z. and Y.Z. All authors have read and agreed to the published version of the manuscript.

Funding: This research was funded by the Shenzhen Science and Technology Program (GJHZ20220913142605010), the Shandong Excellent Young Scientists Fund Program (Overseas) (2022HWYQ-016), the Shandong Provincial Natural Science Foundation (ZR2021QE254), Jinan Lead Researcher Project (202333051), and the Spring Sunshine Program by the Ministry of Education of China (HZKY20220470).

Institutional Review Board Statement: Not applicable.

Informed Consent Statement: Not applicable.

Data Availability Statement: The raw data supporting the conclusions of this article will be made available by the authors on request.

Conflicts of Interest: Kaixing Zhang and Runze Xu were employed by Shandong Hi-Speed Jinan Ring Road West Highway Co., Ltd. Weizhe Feng was employed by Shandong Provincial Communications Planning and Design Institute Group Co., Ltd. The remaining authors declare that the research was conducted in the absence of any commercial or financial relationships that could be construed as a potential conflict of interest.

References

1. Kitazume, M. *The Deep Mixing Method*; CRC Press: Boca Raton, FL, USA, 2013.
2. Bergado, D.T.; Anderson, L.R.; Miura, N.; Balasubramaniam, A.S. *Soft Ground Improvement in Lowland and Other Environments*; ASCE Press: Reston, VA, USA, 1996.
3. Al-Tabbaa, A. Soil mixing in the UK 1991–2001: State of practice report. In *Ground Improvement*; Institution of Civil Engineers: London, UK, 2003.
4. Bell, F. *Engineering Treatment of Soils*; CRC Press: London, UK, 1993.
5. Porbaha, A. State of the art in deep mixing technology: Part I. Basic concepts and overview. *Proc. Inst. Civ. Eng. Ground Improv.* **1998**, *2*, 125–139. [CrossRef]
6. Diamond, S.; Kinter, E.B. *Mechanisms of Soil-Lime Stabilization*; U. S. Bureau of Public Roads: Washington, DC, USA, 1996; Volume 33, pp. 260–265.
7. Jamsawang, P.; Bergado, D.T.; Voottipruex, P. Field behaviour of stiffened deep cement mixing piles. *Proc. Inst. Civ. Eng.-Ground Improv.* **2011**, *164*, 33–49. [CrossRef]
8. Srijaroen, C.; Hoy, M.; Horpibulsuk, S.; Rachan, R.; Arulrajah, A. Soil-cement screw pile: Alternative pile for low-and medium-rise buildings in soft Bangkok clay. *J. Constr. Eng. Manag.* **2021**, *147*, 04020173. [CrossRef]
9. Yi, Y.; Liu, S.; Du, Y.; Zhu, Z.; Du, G. The T-Shaped Deep Mixed Column Application in Soft Ground Improvement. In Proceedings of the International Conference on Grouting & Deep Mixing, New Orleans, LA, USA, 15–18 February 2012.
10. Liu, L.; Zhou, A.; Deng, Y.; Cui, Y.; Yu, Z.; Yu, C. Strength performance of cement/slag-based stabilized soft clays. *Constr. Build. Mater.* **2019**, *211*, 909–918. [CrossRef]
11. Liu, L.; Deng, T.; Deng, Y.; Zhan, L.; Horpibulsuk, S.; Wang, Q. Stabilization nature and unified strength characterization for cement-based stabilized soils. *Constr. Build. Mater.* **2022**, *336*, 127544. [CrossRef]
12. Taki, O.; Yang, D.S. Soil-Cement Mixed Wall Technique. In Proceedings of the Geotechnical Engineering Congress, Boulder, CO, USA, 10–12 June 1991.
13. He, L. Spatial Variability in Deep Soil Mixing—Centrifuge Model and Field Data Study. Ph.D. Thesis, National University of Singapore, Singapore, 2018.
14. He, W.-X.; Shen, X.-D. Mechanical behavior of soil-sand-cement admixture. *Rock Soil Mech.* **2011**, *32*, 392–396.
15. Yapage, N.N.S.; Liyanapathirana, D.S. A parametric study of geosynthetic-reinforced column-supported embankments. *Geosynth. Int.* **2014**, *21*, 213–232. [CrossRef]
16. Zhuang, Y.; Wang, K.Y. Finite-Element Analysis on the Effect of Subsoil in Reinforced Piled Embankments and Comparison with Theoretical Method Predictions. *Int. J. Geomech.* **2016**, *16*, 04016011. [CrossRef]
17. Ariyarathne, P.; Liyanapathirana, D.S.; Leo, C.J. Comparison of Different Two-Dimensional Idealizations for a Geosynthetic-Reinforced Pile-Supported Embankment. *Int. J. Geomech.* **2013**, *13*, 754–768. [CrossRef]
18. Ariyarathne, P.; Liyanapathirana, D.S. Review of existing design methods for geosynthetic-reinforced pile-supported embankments. *Soils Found.* **2015**, *55*, 17–34. [CrossRef]
19. Zhuang, Y.; Ellis, E.A. Finite-element analysis of a piled embankment with reinforcement and subsoil. *Geotechnique. J.* **2016**, *66*, 596–601. [CrossRef]
20. Voottipruex, P.; Suksawat, T.; Bergado, D.; Jamsawang, P. Numerical simulations and parametric study of SDCM and DCM piles under full scale axial and lateral loads. *Comput. Geotech.* **2011**, *38*, 318–329. [CrossRef]
21. King, D.J.; Bouazza, A.; Gniel, J.R.; Rowe, R.K.; Bui, H.H. Serviceability design for geosynthetic reinforced column supported embankments. *Geotext. Geomembr.* **2017**, *45*, 261–279. [CrossRef]
22. Chai, J.-C.; Shrestha, S.; Hino, T.; Ding, W.-Q.; Kamo, Y.; Carter, J. 2D and 3D analyses of an embankment on clay improved by soil–cement columns. *Comput. Geotech.* **2015**, *68*, 28–37. [CrossRef]
23. Zhuang, Y.; Wang, K.Y. Three-dimensional behavior of biaxial geogrid in a piled embankment: Numerical investigation. *Can. Geotech. J.* **2014**, *52*, 1629–1635. [CrossRef]
24. Wang, A.; Zhang, D.; Deng, Y. Lateral response of single piles in cement-improved soil: Numerical and theoretical investigation. *Comput. Geotech.* **2018**, *102*, 164–178. [CrossRef]
25. Zhang, P.; Qi, X.; Ding, H.; Le, C.; Lin, Y.; Xiao, J. Bearing characteristics of mono-column composite bucket foundation in sand for offshore wind turbines. *Ocean. Eng.* **2023**, *280*, 114870. [CrossRef]
26. Wang, K.; Chen, M.; Zhang, R.; Fang, W. Finite element simulation of load bearing capacity of circular CFST long columns with localized corrosion under eccentric load. *Structures* **2022**, *43*, 1629–1642. [CrossRef]
27. Xia, M.; Xu, S.; Wang, Y.; Li, H.; Zhao, B. Experimental study on bearing capacity of corroded Q345 H-shaped steel column under axial compression load. *J. Build. Eng.* **2022**, *52*, 104354. [CrossRef]
28. Mohtasham, M.R.; Khodaparast, M. Investigation of the effect of dimensional characteristics of stone column on load-bearing capacity and consolidation time. *Civ. Eng. J.* **2018**, *4*, 1437–1446. [CrossRef]
29. Zhu, S.; Chen, C.; Cai, H.; Mao, F. Analytical modeling for the load-transfer behavior of stiffened deep cement mixing (SDCM) pile with rigid cap in layer soils. *Comput. Geotech.* **2022**, *144*, 104618. [CrossRef]

30. Jiu, Y.; Gao, Y.; Lei, F.; Zhu, Y.; Zhang, Z. Nonlinear Analysis of Bearing Characteristics of Stiffened Deep Cement Mixing Piles under Vertical Loading. *Buildings* **2024**, *14*, 816. [CrossRef]
31. El Sawwaf, M.; Azzam, W.; Aamer, F.; Abd El Ghaffar, A. Laboratory modelling of stiffened deep mixing columns with variable diameter under vertical load in loose sand. *Int. J. Geotech. Eng.* **2024**, *18*, 554–567. [CrossRef]